*J. Plasma Physics* (2002), *vol.* 68, *part* 4, *pp.* 267–284.  
DOI: 10.1017/S0022377802001964 Printed in the United Kingdom

# Generation of extra and very low-frequency (ELF/VLF) radiation by ionospheric electrojet modulation using high-frequency (HF) heating waves

S. P. KUO

Department of Electrical Engineering, Polytechnic University, Farmingdale, NY, USA
(spkuo@rama.poly.edu)

(Received 3 June 2002)

**Abstract.** Extra and very low-frequency (ELF/VLF) wave generation by modulated polar electrojet currents is studied numerically. Through Ohmic heating by the amplitude-modulated high-frequency heating wave, the conductivity and thus the current of the electrojet are modulated accordingly to set up the ionospheric antenna current. Stimulated thermal instability, which can further enhance the electrojet current modulation, is studied. It is first analysed analytically to determine the threshold heating power for its excitation. The nonlinear evolutions of the generated ELF/VLF waves enhanced by the instability are then studied numerically. Their spectra are also evaluated. The field intensity of the emission at the fundamental modulation frequency is found to increase with the modulation frequency in agreement with the Tromso observations. The efficiency enhancement by the stimulated thermal instability is hampered by inelastic collisions of electrons with neutral particles (mainly due to vibration excitation of $N_2$), which cause this instability to saturate at low levels. However, the electron inelastic collision loss rate drops rapidly to a low value in the energy regime from 3.5 to 6 eV. As the heating power exceeds a threshold level, significant electron heating enhanced by the instability is shown, which indeed causes a steep drop in the electron inelastic collision loss rate. Consequently, this instability saturates at a much higher level, resulting to a near step increase (of about 10–13 dB depending on the modulation wave form) in the spectral intensity of ELF radiation. The dependence of the threshold power of the HF heating wave on the modulation frequency is determined.

## 1. Introduction

In the polar region, an electrojet current appears frequently in the lower ionosphere. This current is driven by a DC space charge field and can be perturbed through perturbations on the background electric conductivity. For example, an amplitude-modulated powerful HF wave modulated at extra and very low frequency (ELF/VLF) can be introduced to heat a background plasma. The HF wave modulates the electron temperature, which results in a modulation of the electron conductivity in a similar fashion to the power modulation of the heating wave. Consequently, the electrojet current driven by the background DC fields become oscillating in time to act virtually as an antenna. The AC part of the current

becomes the source current of ELF/VLF radiation. Experiments (Stubbe et al. 1981, 1982, 1985; Ferraro et al. 1982, 1984; Barr and Stubbe 1984a,b, 1991a,b; James et al. 1984; Rietveld et al. 1986, 1989; Lee et al. 1990; McCarrick et al. 1990; Barr et al. 1991; Villasenor et al. 1996) and theoretical studies (Kuo and Lee 1983; Papadopoulos and Chang 1985; Papadopoulos et al. 1990; Kuo 1993; Kuo and Lee 1993; Stubbe and Kopka 1997; Kuo et al. 1998, 2000) on ELF/VLF wave generation by such an approach in the high-latitude ionosphere have been pursued over the past two decades. The frequencies of radiation are easily controlled by the modulation frequencies of amplitude-modulated HF heating waves. However, the generation efficiency and signal quality are critical to practical applications.

A beam-painting approach (Papadopoulos et al. 1990) that enlarges the modulated region of the electrojet to enhance the ionospheric antenna gain has been suggested. However, experiments (Barr and Stubbe 1991a,b) indicated that using a beam-painting approach to enhance the ELF/VLF radiation efficiency would require the heating facility to operate at a considerably higher power level than that of the Tromso heating facility. Kuo and Lee (1993) and Kuo (1993) then showed that in addition to the conventional electrojet modulation process via the passive Ohmic heating mechanism, an active process by exciting stimulated thermal instability could provide a more effective modulation on the electrojet. The thermal instability is excited because the increasing dependence of the elastic electron–neutral collision frequency $\nu_{\rm en}$ on the electron temperature $T_e$, i.e. $\nu_{\rm en} \propto T_e^{5/6}$, provides a positive feedback channel to enhance electron heating by the HF heating wave. The thermal instability leads to a transient temperature response from the electrojet plasma, caused by Ohmic heating of the modulated HF wave, which grows exponentially at the expense of the free energy of the HF wave as well as the background electrojet current, further enhancing the modulation of the electrojet current for ELF wave generation. The results of the numerical and analytical analyses (Kuo et al. 1998, 2000) further indicate that the signal quality and the generation efficiency depend on the mode type (O or X) of the HF wave, modulation scheme and modulation frequency. Moreover, the theoretical analysis (Kuo et al. 2000) also shows that stimulated thermal instability can, in fact, be a dominant process in electron temperature modulation before the nonlinear damping process of inelastic collisions stabilizes it.

The inelastic collision frequency of electrons (e.g. vibration excitation of $N_2$ and $O_2$) has a strong dependence on the electron temperature. It starts with a rapidly increasing dependence in the low electron temperature regime. This increasing dependence on the electron temperature slows down as the electron temperature increases further. The data curve presented in Fig. 5 on page 57 of Gurevich's book (Gurevich 1978) shows that the inelastic collision cross-section of the electron, after reaching a peak at about 2.5 eV of the electron temperature (i.e. the electron energy at about 3.5 eV), decreases rapidly with a further increase of the electron temperature. It stays at low values for $2.5 < T_e < 4.5$ eV before the optical excitation and ionization processes become significant. It suggests that the saturation level of stimulated thermal instability should be enhanced drastically by increasing electron heating to exceed a critical rate (Kuo et al. 2002).

In the present work, the refined electron thermal energy equation that governs the nonlinear evolution of the stimulated thermal instability is analysed numerically for a general power modulation function of the HF heating wave. The relationship between the radiation field and the electron temperature modulation

in the electrojet current is derived in Sec. 2. The modal equations for analytical and numerical analyses are derived in Sec. 3, in which the derivation of the electron energy loss rate owing to inelastic collisions (including ionization) is presented. Presented in Sec. 4 is a linear stability analysis to explore the threshold condition and growth rate of the stimulated thermal instability excited by the amplitude-modulated HF heating wave. In Sec. 5, numerical results showing the dependence of the temporal and spectral distributions of the electron temperature modulation and ELF/VLF radiation on the modulation scheme, modulation frequency and heating power, is presented. Conclusions are finally drawn in Sec. 6.

## 2. Current modulation and radiation field

The polar electrojet current is driven by a DC electric field $\mathbf{E}_0 = \hat{\mathbf{x}}E_0$ in the collisional plasma, which is embedded in a background magnetic field $\mathbf{B}_0 = -\hat{\mathbf{z}}B_0$. It consists of a Pederson and Hall current. The Pederson current flows in the $x$-direction (i.e. in the same direction as the driving field) and the Hall current flows in the $y$-direction. It is owing to collisions in the plasma that the current is able to flow in directions perpendicular to the background magnetic field. Thus, the electrojet current depends on the collision frequencies of the plasma. This explains why the electrojet current appears only in E and D regions, rather than the F region, of the ionosphere. Therefore, the electrojet current can be modulated through plasma collision frequencies, which are generally temperature dependent. Using powerful HF waves, electron heating is much more effective than ion heating. Hence, only the electron electrojet current modulation has to be considered. The electron drift velocity is given by

$$\mathbf{u}_e = -(eE_0/m)(\hat{\mathbf{x}}\nu_{\rm en} - \hat{\mathbf{y}}\Omega_e)/\left(\nu_{\rm en}^2 + \Omega_e^2\right), \tag{1}$$

where $\nu_{\rm en}$ and $\Omega_e$ are the elastic electron–neutral collision frequency and electron cyclotron frequency, respectively.

Then the electron electrojet current density is obtained to be

$$\mathbf{J}_e = -en_0\mathbf{u}_e = (n_0e^2E_0/m)(\hat{\mathbf{x}}\nu_{\rm en} - \hat{\mathbf{y}}\Omega_e)/\left(\nu_{\rm en}^2 + \Omega_e^2\right). \tag{2}$$

In (2), $\nu_{\rm en} \propto T_e^{5/6}$; hence, the electron electrojet current can be modulated through either the electron density $n_0$ or electron temperature $T_e$. Since the ionization process requires much more HF power than that for the heating process, presently electrojet current modulation in HF heating experiments is mainly through modulated electron heating approach. The induced time-varying current density $\mathbf{J}_{\rm ac}$ in the electrojet is a source of radiation with a vector potential $\mathbf{A}(\mathbf{r}, t)$ that satisfies the inhomogeneous wave equation

$$\left(c^2\nabla^2 - \partial_t^2\right)\mathbf{A} = -\mu_0c^2\mathbf{J}_{\rm ac}, \tag{3}$$

where the plasma effect on the propagation of radiation is neglected. Equation (3) is solved, with the aid of the retarded Green function, to obtain a 'retarded solution'

$$\mathbf{A}(\mathbf{r}, t) = (\mu_0/4\pi)\int d\mathbf{r}'\int dt'\,[\mathbf{J}_{\rm ac}(\mathbf{r}', t')/|\mathbf{r} - \mathbf{r}'|]\delta(t' + |\mathbf{r} - \mathbf{r}'|/c - t). \tag{4}$$

The induced current element in the electrojet behaves as a Hertzian dipole, the integrations on the right-hand side (RHS) of (4) can be carried out analytically.

https://doi.org/10.1017/S0022377802001964 Published online by Cambridge University Press

The result determines the radiation field at the receiver, through the relation

$$\mathbf{E}(\mathbf{r},t) = -\partial_t \mathbf{A}, \text{ to be}$$

$$\mathbf{E}(r,t) = -\left(5\omega_{pe}^2 V E_0/24\pi c^2 r\right)\left\{\left[\hat{\mathbf{x}}\left(\Omega_e^2 - \nu_{\text{en}}^2\right) - \hat{\mathbf{y}}2\Omega_e\nu_{\text{en}}\right]/\left(\nu_{\text{en}}^2 + \Omega_e^2\right)^2\right\}(\nu_{\text{en}}/T_e)\partial_t T_e, \tag{5}$$

where $V$ is the effective volume of the source region; $T_e = T_e(t - r/c)$ and $r$ is the distance from the source region to the location of the receiver. Equation (5) shows that electron temperature modulation is the key to using an electrojet for ELF/VLF generation.

## 3. Modal equations

In the presence of HF heating, the electron thermal energy equation (Braginskii 1965; Gurevich 1978) is given by

$$\partial T_e/\partial t + (2T_e/3)\nabla\cdot\mathbf{v}_e + \delta(T_e)\nu_e(T_e)(T_e - T_n) + \text{ionization loss} = (2/3n_0)(Q + \nabla\cdot\mathbf{K}_e\cdot\nabla T_e) + \text{solar heat input}, \tag{6}$$

where $n_0$ is the plasma density, $\mathbf{v}_e$ is the electron fluid velocity, $\delta(T_e)$ is the average relative energy fraction lost in each collision, $\nu_e(T_e)$ is the effective collision frequency of electrons with neutral particles, $T_n$ is the temperature of the background neutral particles. The ionization loss becomes significant as electrons are heated up to high temperature; $Q$ is the total Ohmic heating power density in the background plasma and contributed by the electrojet current and the HF heater wave, $\mathbf{K}_e$ is the thermal conduction tensor and $m$ is the electron mass. The explicit expression of the ionization loss term on the left-hand side (LHS) of (6) will be given later, which may not be ignored in the strong heating cases where the electron temperature can become high enough to contribute significant thermal ionization. Let $T_{e0}$ be the equilibrium electron temperature in the absence of the heating wave and substitute them into (6), the solar source power $\delta(T_{e0})\nu_e(T_{e0})(T_{e0} - T_n) - \frac{2}{3}(Q_{e0}/n_0)$ is determined, where $Q_{e0}$ is the power density contributed by the electron electrojet current. Since only temporal modulation is considered, the two terms involving spatial derivatives on each side of (6) are set to zero.

The total Ohmic heating power density is given by

$$Q = \left\langle J_{et}^2/\sigma\right\rangle \cong \nu_{\text{en}} n_0 m\left[u_e^2 + \langle|v_{pe}|^2\rangle\right], \tag{7}$$

where $\mathbf{J}_{et} = -en(\mathbf{u}_e + \mathbf{v}_{pe})$ is the total electron current density in the background plasma carrying an electrojet and interacting with the HF wave fields, angled brackets indicate the time average over the HF wave period and $\sigma = n_0 e^2/m\nu_{\text{en}}$ is the conductivity of the plasma responsible for the Ohmic loss; $\mathbf{u}_e$ is given by (1).

Considering the electrojet modulation by an X-mode heating wave, which has been shown (Kuo et al. 1998) to be more effective than an O-mode heating wave, the wave electric field of left-hand circular polarization is expressed as $\mathbf{E}_p = (\hat{\mathbf{x}} - i\hat{\mathbf{y}})(\varepsilon_p/2)\exp[i(k_0 z - \omega_0 t)] + \text{c.c.}$ The linear velocity response of electrons to this wave field is given by $\mathbf{v}_{pe} = -i(\hat{\mathbf{x}} - i\hat{\mathbf{y}})[e\varepsilon_p/2m(\omega_0 - \Omega_e + i\nu_{\text{en}})]\exp[i(k_0 z - \omega_0 t)] + \text{c.c.}$ The power of the HF heating wave is modulated periodically, i.e. $\varepsilon_p^2 = \varepsilon_{p0}^2 M(t)$. The periodic power modulation function $M(t)$ can have a general form as

$$M(t) = \sum_{k=0} M_k \cos k(\omega_1 t + \varphi), \tag{8}$$

https://doi.org/10.1017/S0022377802001964 Published online by Cambridge University Press

where $\omega_1/2\pi = f_1 = 1/T_1$ is the modulation frequency and the same phase $\varphi$ is assumed for all of the harmonic components to simplify the presentation; $M_0 = \langle\varepsilon_p^2\rangle/\varepsilon_{p0}^2$ is the ratio of the average power to the peak power. Thus, $u_e = eE_0/m(\nu_{\text{en}}^2 + \Omega_e^2)^{1/2}$ and $\langle|v_{pe}|^2\rangle = v_q^2 M(t)$ will be used to express (7) explicitly, where $v_q^2 = (e\varepsilon_{p0}/m)^2/[(\omega_0 - \Omega_e)^2 + \nu_{\text{en}}^2]$.

To obtain an explicit expression of (6), the two energy loss terms on the LHS of (6) have to be derived. Based on Gurevich (1978), their derivations are summarized as follows.

### *3.1. Energy fraction loss rate in each collision*

Both elastic and inelastic collisions contribute to the heat loss. The main processes involved in the inelastic collisions in the energy regime of interest ($< 6\,\text{eV}$) are the rotational and vibration excitation of $N_2$ and $O_2$. Loss through optical excitation processes is neglected and the ionization loss will be considered separately. Thus the fractional electron heat loss rate through collisions with neutral particles can be written as $\delta(T_e)\nu_e(T_e) = (\delta_{\text{el}} + \delta_r + \delta_v)\nu_e$, i.e. the sum of the three main contributions from the elastic collision, rotational excitation and vibrational excitation, respectively.

1. Elastic collision (Gurevich 1978, p. 62)

$$\delta_{\text{el}}\nu_e = (2m/M_n)\nu_{\text{en0}}(T_e/T_{e0})^{5/6} = (2m/M_n)\nu_{\text{en0}}\chi^{5/6},$$

where $\nu_{\text{en0}} = \nu_{\text{en}}(T_{e0}) = (4 \times 2^{5/6}/3\pi^{1/2})CN_m(T_{e0}/m)^{5/6}\Gamma(\frac{10}{3})$; $T_{e0}$ is the unperturbed electron temperature and $C = 3.5 \times 10^{-16}\,\text{cm}^2\ (10^7\,\text{cm s}^{-1})^{-2/3}$; $2m/M_n = 3.623 \times 10^{-5}$; and $\chi = T_e/T_{e0}$.

2. Rotational excitation (Gurevich 1978, pp. 52–54, 64 and 2.123 and 2.143b)

$$\begin{aligned}\delta_r\nu_e &= \left(16 \times 2^{1/2}/3\pi^{1/2}\right)B_0\sigma_0 N_m/(T_e m)^{1/2} \\ &= (2m/M_n)\nu_{\text{en0}}(T_e/T_{e0})^{-1/2}\left[2^{2/3}M_n B_0\sigma_0/m^2(T_{e0}/m)^{4/3}C\Gamma\left(\tfrac{10}{3}\right)\right],\end{aligned}$$

where $\sigma_0 = 8\pi Q^2 a_0^2/15$ and $B_0 Q^2 = 3.3 \times 10^{-4}\,\text{eV}$; $a_0 = h^2/m(2\pi e)^2 \cong 5.29 \times 10^{-9}\,\text{cm}$, and thus $B_0\sigma_0 = (8\pi/15)a_0^2 B_0 Q^2 = 1.547 \times 10^{-20}\,\text{eV cm}^2$. For $T_{e0} = 1500\,\text{K} = 0.1293\,\text{eV}$, we have $\delta_r\nu_e = 8.38 \times (2m/M_n)\nu_{\text{en0}}\chi^{-1/2}$.

3. Vibrational excitation (Gurevich 1978, pp. 54–56, 2.134 and 2.144, and Table 4)

$$\delta_v\nu_e = (16\pi N_m/3Nm^2T_e)\sum \varepsilon_v\varepsilon_v^k\sigma_v^k f_{00}\left(\varepsilon_v^k\right),$$

where $f_{00}(\varepsilon_v^k) = N(m/2\pi T_e)^{3/2}\exp(-\varepsilon_v^k/T_e)$. Thus,

$$\begin{aligned}\delta_v\nu_e &= \left[8N_m/3(2\pi)^{1/2}m^3\right](T_{e0}/m)^{-5/2}\chi^{-5/2}\sum \varepsilon_v\varepsilon_v^k\sigma_v^k\exp\left[-\left(\varepsilon_v^k/T_{e0}\right)/\chi\right] \\ &= (2m/M_n)\nu_{\text{en0}}\left[(M_n/2m)(2T_{e0}/m)^{-1/3}/\Gamma\left(\tfrac{10}{3}\right)CT_{e0}^3\right]\chi^{-5/2} \\ &\quad \times \sum \varepsilon_v\varepsilon_v^k\sigma_v^k\exp\left[-\left(\varepsilon_v^k/T_{e0}\right)/\chi\right].\end{aligned}$$

With the aid of $[(M_n/2m)(2T_{e0}/m)^{-1/3}/\Gamma(\frac{10}{3})CT_{e0}^3] = 0.795 \times 10^{22}\,\text{cm}^{-2}\,\text{eV}^{-3}$ and $\sum \varepsilon_v\varepsilon_v^k\sigma_v^k\exp[-(\varepsilon_v^k/T_{e0})/\chi] \cong \{[124e^{-15.78/\chi} + 265e^{-17.4/\chi} + 178e^{-18.7/\chi} + 410.5e^{-22.5/\chi}]$ (from $N_2$) $+ [0.72e^{-4.65/\chi} + 5e^{-9.25/\chi} + 4.36e^{-12.89/\chi}]$ (from $O_2$)$\} \times$

https://doi.org/10.1017/S0022377802001964 Published online by Cambridge University Press

$10^{-18}\,\mathrm{cm}^2\,\mathrm{eV}^3$, leads to

$$\begin{aligned}\delta_v\nu_e &= 0.795\times10^4(2m/M_n)\nu_{\mathrm{en}0}\chi^{-5/2}\big[0.72e^{-4.65/\chi}+5e^{-9.25/\chi}+4.36e^{-12.89/\chi}\\ &\quad+124e^{-15.78/\chi}+265e^{-17.4/\chi}+178e^{-18.7/\chi}+410.5e^{-22.5/\chi}\big]\\ &= 0.99\times10^6(2m/M_n)\nu_{\mathrm{en}0}\chi^{-5/2}\big[5.8\times10^{-3}e^{-4.65/\chi}+4\times10^{-2}e^{-9.25/\chi}\\ &\quad+8.75\times10^{-3}e^{-12.89/\chi}+e^{-15.78/\chi}+2.14e^{-17.4/\chi}\\ &\quad+1.44e^{-18.7/\chi}+3.31e^{-22.5/\chi}\big]\\ &= (2m/M_n)\nu_{\mathrm{en}0}\chi^{-5/2}\big[54.73e^{4.65(1-1/\chi)}+3.82e^{9.25(1-1/\chi)}\\ &\quad+8.75\times10^{-2}e^{12.89(1-1/\chi)}+0.138e^{15.78(1-1/\chi)}+5.85\times10^{-2}e^{17.4(1-1/\chi)}\\ &\quad+1.07\times10^{-2}e^{18.7(1-1/\chi)}+5.52\times10^{-4}e^{22.5(1-1/\chi)}\big].\end{aligned}$$

Therefore, we obtain

$$\delta(T_e)\nu_e(T_e)\cong(2m/M_n)\nu_{\mathrm{en}0}\big[\chi^{5/6}+8.38\chi^{-1/2}+\mu_I(\chi)\big], \tag{9}$$

where

$$\begin{aligned}\mu_I(\chi) &= \chi^{-5/2}\big[14.73e^{6.98(1-1/\chi)}+0.1e^{13.88(1-1/\chi)}+3.81\times10^{-4}e^{19.34(1-1/\chi)}\\ &\quad+1.43\times10^{-4}e^{23.67(1-1/\chi)}+2.7\times10^{-5}e^{26.1(1-1/\chi)}\\ &\quad+2.59\times10^{-6}e^{28.05(1-1/\chi)}+3.54\times10^{-7}e^{30.87(1-1/\chi)}\big].\end{aligned} \tag{10}$$

It is noted that (9) is a simplified expression obtained by regrouping original exponential terms contributed by the dominant excitation states given in Table 4 of Gurevich (1978). The cross-sections for the excitation of optical levels and for the dissociation of molecules in air become significant in much larger electron energy regimes, which do not overlap with that dominating with vibration excitation as shown in Fig. 1. Thus, the fractional electron heat losses through these two inelastic collision processes will be neglected in the following analysis.

### *3.2. Ionization loss*

Electrons in plasma have a velocity distribution and those energetic electrons in the tail portion of the distribution can ionize the background neutral particles. However, the distribution decays exponentially with the electron energy and the ionization frequency is very small under the normal low electron temperature situation. When the heating wave is introduced, more energetic electrons are produced and the electron ionization frequency can increase considerably. Applying the formulations and parameters given in Gurevich (1978), the ionization frequency is derived as follows.

The electron energy thermalization time is proportional to $\nu_{\mathrm{en}}^{-1}$, which is much shorter than the modulation period of the heating wave. Thus, the bulk of electrons are maintained in a Maxwellian distribution with a time-dependent temperature governed by (6). The heating enhances as well as flattens the electron distribution in the tail region, which is then assumed to have the form $f_0(v) = f_0(v_i)\exp[-\alpha(v-v_i)]$ for $v \geqslant v_i$, the ionization velocity, where $\alpha = mv_i/T_e$ and $f_0(v_i) = n_0(m/2\pi T_e)^{3/2}\exp(-\alpha v_i/2)$. Using the ionization cross-section (Gurevich

https://doi.org/10.1017/S0022377802001964 Published online by Cambridge University Press

1978) defined by (2.174), the integration in (2.173) can be carried out to obtain the ionization frequency $\nu_{\rm ion}$ as

$$\nu_{\rm ion} = (2/\pi)^{1/2}\left[N_m v_i^5 Q/(\alpha_0 v_i)^2 v_{t0}^3\right] D\chi^{1/2}\exp(-\alpha_0 v_i/2\chi),$$

where $N_m$ is the density of the neutral gas, $\alpha_0 v_i = (v_i/v_{t0})^2$, $v_{t0} = (T_{e0}/m)^{1/2}$, $Q$ is proportional to the ionization cross-section and $D = 1 + 6\chi/\alpha_0 v_i + 18(\chi/\alpha_0 v_i)^2 + 24(\chi/\alpha_0 v_i)^3$.

We now use the values for $Q$ and $v_i$ given by (2.175) of Gurevich (1978) and the densities of $O_2$ and $N_2$ at 100 km altitude, i.e. $N_m = 3.5 \times 10^{17}\,\mathrm{m}^{-3}$ for $O_2$ and $1.4 \times 10^{18}\,\mathrm{m}^{-3}$ for $N_2$, the ionization frequencies for $O_2$ and $N_2$ are expressed explicitly as

$$\nu_{\rm ion}(O_2) = 4.3 \times 10^2 D_1 \chi^{1/2} e^{-94.3/\chi}$$

and

$$\nu_{\rm ion}(N_2) = 1.57 \times 10^3 D_2 \chi^{1/2} e^{-121.7/\chi},$$

where $T_{e0} = 1500\,\mathrm{K}$, i.e. $v_{t0} = 1.5 \times 10^5\,\mathrm{m\,s^{-1}}$, is assumed; $D_1 = (1 + 0.032\chi + 5 \times 10^{-4}\chi^2 + 3.6 \times 10^{-6}\chi^3)$ and $D_2 = (1 + 0.025\chi + 3 \times 10^{-4}\chi^2 + 1.7 \times 10^{-6}\chi^3)$.

Thus, the electron energy loss rate due to the ionization process is given by

$$\nu_{\rm ion}\varepsilon = \nu_{\rm ion}(O_2)\varepsilon_i(O_2) + \nu_{\rm ion}(N_2)\varepsilon_i(N_2), \tag{11}$$

where $\varepsilon_i(O_2)$ and $\varepsilon_i(N_2)$ are the ionization energies of $O_2$ and $N_2$, which are 12.1 eV $\cong 93T_{e0}$ and 15.6 eV $\cong 120T_{e0}$, respectively.

Equations (5) and (6) are the modal equations to be solved numerically for the dependence of the ELF/VLF radiation intensity on the power and modulation scheme of the X-mode HF heating wave.

## 4. Thermal instability

The conventional electrojet modulation process is via the passive Ohmic heating mechanism. To achieve a more effective modulation on the electrojet current, an active process exciting a stimulated thermal instability is investigated. The mechanism responsible for the excitation of a thermal instability is based on the electron temperature dependence of the elastic electron neutral collision frequency $\nu_{\rm en}$, i.e. $\nu_{\rm en} \propto T_e^{5/6}$. Since the heating rate $\propto \nu_{\rm en}$, a positive feedback channel is thus established.

To show that the modulated heating can lead to a stimulated thermal instability, (6) is solved for a periodic power modulation function (8). Setting $T_e = T_{e0} + \delta T_e$, with $|\delta T_e| \ll T_{e0}$, in (6), and with the aid of (7)–(11), the equation for $\delta T_e$ is obtained to be

$$\left\{d_t + \left[a - b\sum_{k=0} M_k \cos k(\omega_1 t + \varphi)\right]\right\}\delta T_e = \frac{6}{5} b T_{e0} \sum_{k=0} M_k \cos k(\omega_1 t + \varphi), \tag{12}$$

where $a = \frac{5}{9}\nu_{\rm en0}[230(m/M_n)(1.38 - T_n/T_{e0}) - u_0^2/v_{te}^2]$ and $b = \frac{5}{9}\nu_{\rm en0}(v_q/v_{te})^2$; $u_0 = u_e(T_{e0})$; the ionization effect is not included in the analysis.

https://doi.org/10.1017/S0022377802001964 Published online by Cambridge University Press

Introducing $\delta T_e = \Psi \exp[\gamma t + \sum_{k=1} \beta_k \sin k(\omega_1 t + \varphi)]$, where $\gamma = bM_0 - a$ and $\beta_k = bM_k/k\omega_1$, into (12), leads to

$$d_t \Psi = \frac{6}{5} bT_{e0} \exp\left[-\sum_{k=1} \beta_k \sin k(\omega_1 t + \varphi)\right] \exp(-\gamma t) \sum_{k=0} M_k \cos k(\omega_1 t + \varphi), \quad (13)$$

where the exponential function $\exp[-\sum_{k=1} \beta_k \sin k(\omega_1 t + \varphi)]$ can be converted by the Bessel function expansion into a sum of harmonic functions for integration. Since $|\beta_k| \ll |\beta_1|$ for $k \geqslant 2$, approximations can be made to simplify the expansion of this exponential function to $\exp[-\sum_{k=1} \beta_k \sin k(\omega_1 t + \varphi)] \cong \sum_h [I_h(\beta_1) - U_h] \exp[ih(\omega_1 t + \phi)]$, where $I_h$ is a modified Bessel function of order $h$; $U_h = I_0(\beta_1)\beta_h e^{-ih\pi/2}/2i$ for $|h| \geqslant 2$ and $U_0 = U_{\pm 1} = 0$; $U_{-h} = (-1)^{h+1} U_h$; $h$ runs from $-\infty$ to $\infty$ and $\phi = \varphi + \pi/2$. Thus (13) can be integrated to be

$$\psi = \psi_0 + \frac{3}{5} bT_{e0} \sum_{k=0} M_k \sum_h [\exp(ih\phi)/(-\gamma + ih\omega_1)](C_{h,k} - iS_{h,k}) \times [\exp(-\gamma t + ih\omega_1 t) - 1], \quad (14)$$

where $C_{h,k} = (\Lambda_{h-k} + \Lambda_{h+k}) \cos(k\pi/2)$, $S_{h,k} = (\Lambda_{h-k} - \Lambda_{h+k}) \sin(k\pi/2)$, $\Lambda_p = I_p(\beta_1) - U_p$; $\psi_0 = \psi(t = 0)$ is determined from the initial condition $\langle \delta T_e \rangle = 0$ at $t = 0$ to be

$$\psi_0 = \frac{3}{5} bT_{e0} \sum_{k=0} \sum_h [M_k/(-\gamma + ih\omega_1)] \{\exp(ih\phi) - [(-1)^h I_h - U_h]/I_0\} (C_{h,k} - iS_{h,k}). \quad (15)$$

Therefore, with the aid of (14) and (15), the temperature perturbation is obtained,

$$\delta T_e \cong \sum_n [\delta T_{sn} + \delta T_{tn} \exp(\gamma t)] \exp[in(\omega_1 t + \phi)], \quad (16)$$

where $\delta T_{sn}$ and $\delta T_{tn}$ are given by

$$\delta T_{sn} = \frac{3}{5} bT_{e0} \sum_{k=0} \sum_h [M_k/(-\gamma + ih\omega_1)](C_{h,k} - iS_{h,k}) [(-1)^{h-n} I_{h-n} + U_{h-n}]$$
$$\cong (-i)^n \frac{3}{5} bT_{e0} I_0 [M_n/(-\gamma + in\omega_1)][I_0 + (-1)^n \Lambda_{2n}]$$

and

$$\delta T_{tn} = -\frac{3}{5} bT_{e0} \sum_{k=0} \sum_h [M_k/(-\gamma + ih\omega_1)](C_{h,k} - iS_{h,k}) [(-1)^n I_n + U_n] \times [(-1)^h I_h - U_h]/I_0 \cong \frac{6}{5} bT_{e0} I_0 (M_0/\gamma) [(-1)^n I_n + U_n]. \quad (17)$$

The first term on the RHS of (16) has constant-amplitude $\delta T_{sn}$ for each harmonic component and is the steady-state response of the plasma to the HF input. The second term is contributed by the transient response of the plasma to the modulated heating and, as shown, its amplitude grows exponentially in time with a growth rate $\gamma$. The initial amplitude $\delta T_{tn}$ of each harmonic component of the transient response is governed by the HF input, rather than by the background noise. It manifests a stimulated thermal instability, which enhances the electron

https://doi.org/10.1017/S0022377802001964 Published online by Cambridge University Press

temperature modulation at the expense of the free energy of the HF heating wave as well as the background electrojet current.

The growth rate $\gamma$ of this instability is calculated by using the following E region parameters: $T_n \cong T_i = 300\,\mathrm{K}$, $T_{e0} = 1500\,\mathrm{K}$, $\nu_{\mathrm{en}0} = 5 \times 10^4\,\mathrm{s}^{-1}$, $M_n(\mathrm{NO})/m = 5.52 \times 10^4$, $\Omega_e/2\pi = 1.35\,\mathrm{MHz}$, $v_{te} = 1.5 \times 10^5\,\mathrm{m\,s}^{-1}$ and $E_0 = 50\,\mathrm{mV\,m}^{-1}$, and choosing $\omega_0/2\pi = 4.04\,\mathrm{MHz}$. It is given by $\gamma = 133.5[\varepsilon_{p0}^2 M_0 - 1]\,\mathrm{s}^{-1}$. Thus, the instability threshold is found to be $\varepsilon_{p0\mathrm{th}} = 1/\sqrt{M_0}\,\mathrm{V\,m}^{-1}$, where $M_0$ is the ratio of the average heating power to the peak power. For example, for 50% rectangular wave modulation, $M_0 = \frac{1}{2}$ and $\varepsilon_{p0\mathrm{th}} = \sqrt{2}\,\mathrm{V\,m}^{-1}$. This field amplitude can be exceeded by the radiation field of the European Incoherent Scatter (EISCAT) facility's superheater (Stubbe 1996) in Tromso, Norway under a low anomalous absorption condition. It is noted that these are the results of a linear stability analysis. The instability is expected to saturate rapidly by the nonlinear damping from inelastic collisions, which depend strongly on the electron temperature.

The results in (17) indicate that each steady-state harmonic component of the temperature modulation is mainly governed by the corresponding harmonic component of the power modulation function. However, the transient part of the temperature modulation also depends on the DC component of the power modulation function. From (17), we obtain the ratio

$$|\delta T_{tn}/\delta T_{sn}| = (2 - \delta_{n,1}) M_0 b\left(\gamma^2 + n^2\omega_1^2\right)^{1/2}/n\omega_1\gamma \qquad \text{for } n \geqslant 1. \tag{18}$$

This ratio is of the order of 1. It suggests that the stimulated instability is the dominant temperature modulation process. The instability process can significantly improve the efficiency of temperature modulation if the nonlinear damping of the instability caused by inelastic collisions of electrons with neutral particles can be reduced.

Using (5) and (16), with the aid of (17), the induced wave electric field is determined. The wave electric field also consists of a steady-state part and an unstable part. Each part is a summation of harmonics. The result is used to determine the ratio of the harmonic component to the fundamental component for each part of the wave electric field. The ratios for the steady-state response part and for the unstable part are:

$$|E_{sn}/E_{s1}| = (nM_n/M_1)\left(\gamma^2 + \omega_1^2\right)^{1/2}/\left(\gamma^2 + n^2\omega_1^2\right)^{1/2} \qquad \text{for } n \geqslant 2$$

$$|E_{tn}/E_{t1}| = (2M_n/nM_1)\left(\gamma^2 + n^2\omega_1^2\right)^{1/2}/\left(\gamma^2 + \omega_1^2\right)^{1/2} \quad \text{for } n \geqslant 2. \tag{19}$$

The results in (19) also suggest that a better quality signal (i.e. containing fewer harmonic components) is generated if an amplitude modulation scheme producing less harmonic components in the power modulation function is employed.

## 5. Numerical analysis

The numerical analysis will be carried out for electrojet modulation in the region near 100 km altitudes. The heating wave frequency of $\omega_0/2\pi = 4\,\mathrm{MHz}$ is used and E region parameters adopted are $T_n \cong T_i \cong 300\,\mathrm{K}$, $T_{e0} \cong 1500\,\mathrm{K}$, $\nu_{\mathrm{en}0} = 5 \times 10^4\,\mathrm{s}^{-1}$, $E_0 = 50\,\mathrm{mV\,m}^{-1}$, $M_n/m = 5.52 \times 10^4$, $\Omega_e/2\pi = 1.35\,\mathrm{MHz}$ and $v_{t0} = (T_{e0}/m)^{1/2} = 1.5 \times 10^5\,\mathrm{m\,s}^{-1}$. It is noted that in the strong heating power regime the numerical results are insensitive to the initial value of the electron temperature.

In the numerical analysis, dimensionless variables and parameters are introduced: $\chi = T_e/T_{e0}$ as defined previously, $\nu_{\mathrm{en}}/\nu_{\mathrm{en}0} = \chi^{5/6}$, $\tau = \nu_{\mathrm{en}0}t/100$, $R =$

https://doi.org/10.1017/S0022377802001964 Published online by Cambridge University Press

$(\nu_{en0}/100c)r$, $\xi = \tau - R$, $\varepsilon(\xi) = |\mathbf{E}(z,t)/E_0|$, $\omega_{10} = 100\omega_1/\nu_{en0}$, $T_n/T_{e0} = 0.2$, $\eta = (eE_0/m\Omega_e v_{t0})^2$, $b = (\nu_{en0}/\Omega_e)^2$, $\beta = \frac{5}{6} \times 10^{-4}(\omega_{pe}^2\nu_{en0}^3 A_0/4\pi c^2\Omega_e^2)$ and $q = \alpha M(t)$, where $\alpha = (v_q/v_{t0})^2$, $v_q = 1.04 \times 10^4 \varepsilon_{p0}\,\mathrm{m\,s^{-1}}$, $\varepsilon_{p0}$ is in $\mathrm{V\,m^{-1}}$ and $c$ is the speed of light in vacuum. With $\varepsilon_{p0} = \varepsilon_0 = 2.5\,\mathrm{V\,m^{-1}}$ chosen as a reference field amplitude, leads to $v_{q0} = 2.6 \times 10^4\,\mathrm{m\,s^{-1}}$, $\alpha_0 = \alpha(v_q = v_{q0}) = 0.03$ and $\alpha = 0.03p$, where $p = (\varepsilon_{p0}/\varepsilon_0)^2$ is the heating wave power normalized to the reference power.

Thus (5) and (6) are normalized to the dimensionless forms

$$\varepsilon(\xi) = \sqrt{2}\beta\{\chi^{-1/6}(\xi)/[1 + b\chi^{5/3}(\xi)]\}(d/d\tau)\chi(\xi) \tag{20}$$

and

$$\begin{aligned} d\chi/d\tau + 200(m/M_n)[\chi^{5/6} + 8.38\chi^{-1/2} + \mu_I(\chi)](\chi - 0.2) \\ + \chi^{1/2}[0.86D_1(93 + \chi)e^{-94.3/\chi} + 3.14D_2(120 + \chi)e^{-121.7/\chi}] \\ = \tfrac{200}{3}\chi^{5/6}[\eta/(1 + b\chi^{5/3}) + q] + 200[19.3(m/M_n) - \eta/3], \end{aligned} \tag{21}$$

where the spatially dependent terms (i.e. the divergent terms) in (6) have been neglected; the third term on the LHS of (21) is the normalized ionization loss term and the two terms in brackets are contributed from the ionization of $O_2$ and $N_2$, respectively.

### *5.1. Dependence of the radiation intensity on the modulation scheme and frequency*

In the numerical analyses, we first consider the case for a modulation frequency $f_1 = 100\,\mathrm{Hz}$ and for $p = 1$ corresponding to the power transmitted by the Tromso heater prior to being upgraded to a superheater. Equation (21) is solved subject to the initial condition $\chi(0) = 1$. Time functions of modulated electron temperatures produced by X-mode heating waves, which are modulated by the three heater-modulation schemes: (a) sine wave, (b) rectangular wave with a 50% duty cycle and (c) a half-wave-rectified wave, are obtained. The results are then substituted into (20) to obtain the time-dependent radiation fields $\varepsilon(\tau)$ for the three cases. Presented in Figs 1(a)–(c) are the time functions of electron temperatures. As shown, the electron temperature modulations grow very fast but also quickly reach steady states. The saturation levels are determined by the inelastic losses (rotational and vibrational excitations of $N_2$ and $O_2$), which have a strong dependence on the electron temperature as shown by (9) and (10).

The corresponding electric fields $\varepsilon(\tau)$ of emissions are illustrated in Figs 2(a)–(c). Again, the results show that it takes only about one period for signals to reach their respective steady-state levels. Similar to the temperature modulation, the waveforms and steady-state levels of emissions also vary with the modulation schemes. The results show that the field amplitudes produced by the sine wave modulation scheme and by the half-wave rectified wave scheme are the smallest and largest ones, respectively.

Similar calculations for the same three modulation schemes are carried out for a total of six different modulation frequencies: $f_1 = 10$, 50, 100, 500, 1000 and 5000 Hz. The results are then used to show the spectral intensity dependence of emissions on the modulation frequency. The spectral intensity $I_1$ of the fundamental line of the emission, produced by the 100 Hz rectangular pulse modulated heater, is chosen as the reference. The relative spectral intensities $I_1$ and $I_3$ (in dB) of the fundamental lines and the third harmonic lines of emissions as a function of

https://doi.org/10.1017/S0022377802001964 Published online by Cambridge University Press

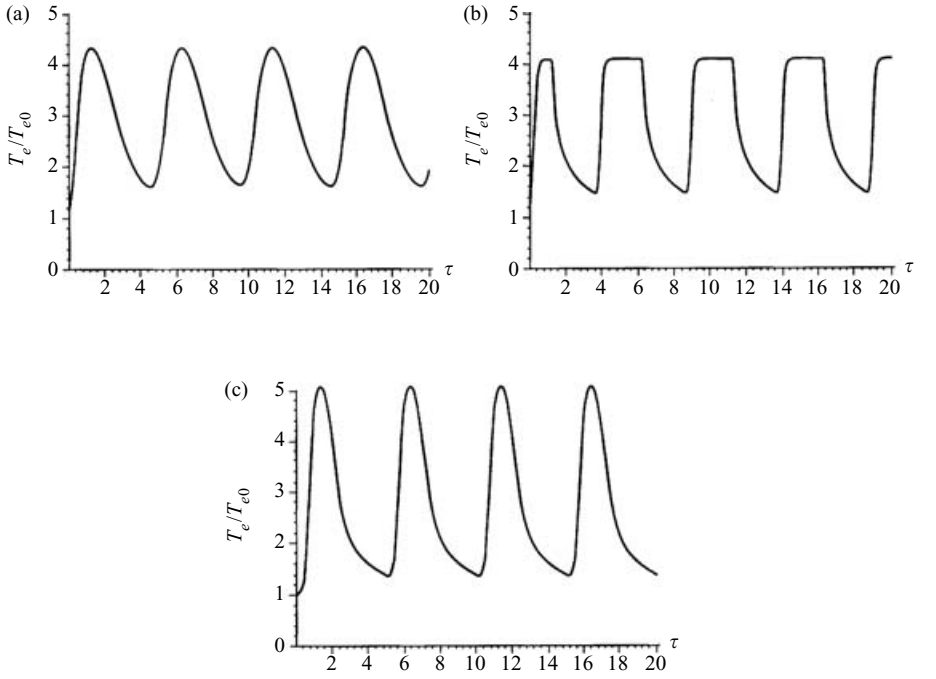


**Figure 1.** Electron temperature modulations induced by: (a) sine wave modulated heater, (b) rectangular wave modulated heater and (c) half-wave-rectified wave modulated heater; X-mode heater and modulation frequency of 100 Hz are used in all cases.

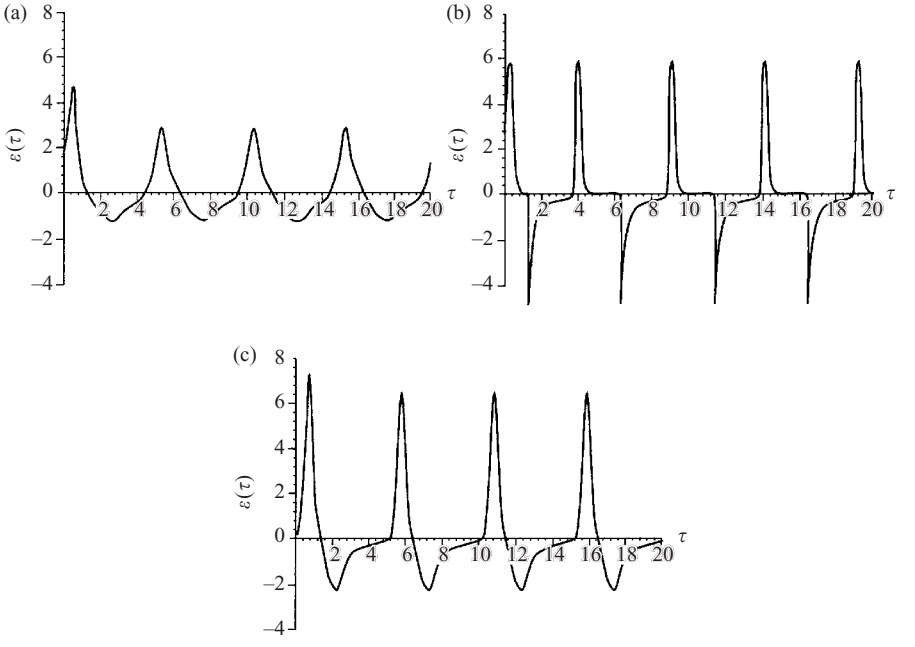


**Figure 2.** Time functions (a)–(c) of the wave fields of ELF emissions corresponding to the temperature modulations presented in Fig. 1.

https://doi.org/10.1017/S0022377802001964 Published online by Cambridge University Press

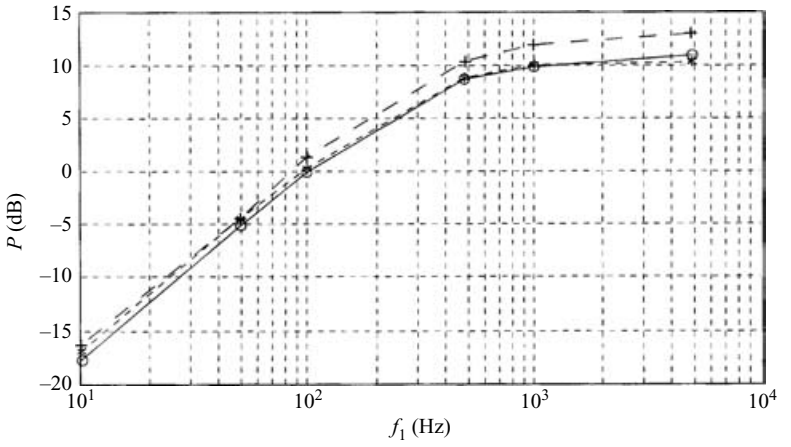


**Figure 3.** The intensities $I_1$ of the fundamental spectral lines of emissions versus the modulation frequency. Curves connecting '○', '+' and '✳' represent emissions produced by the 'sine wave', 'half-wave-rectified wave' and 'rectangular wave' modulated X-mode heater, respectively.

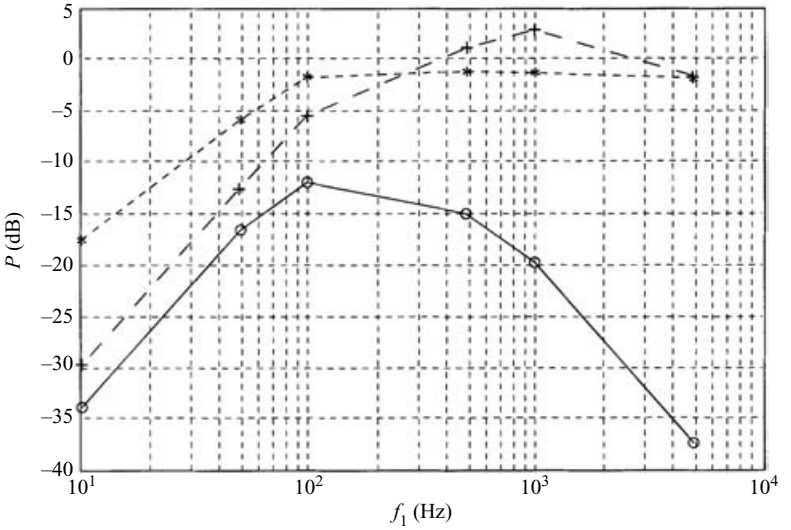


**Figure 4.** A similar dependence for the intensities $I_3$ of the third harmonic lines as that for the fundamental lines presented in Fig. 3.

the modulation frequency are plotted in Figs 3 and 4, respectively. As shown in Fig. 3, the spectral intensities $I_1$ of fundamental lines have a similar dependence on the modulation frequency. They increase considerably in the interval from 10 to 1000 Hz and keep relatively constant values from 1000 to 5000 Hz. On the other hand, the dependence of the spectral intensities $I_3$ of the third harmonic lines shown in Fig. 4 is quite different for the three modulation schemes. In the sine wave case, the spectral intensities of the third harmonic lines increase first with the modification frequency (from 10 to 50 Hz) and then drop quickly to noise levels. The corresponding one produced by the rectangular pulse modulation scheme keeps

https://doi.org/10.1017/S0022377802001964 Published online by Cambridge University Press

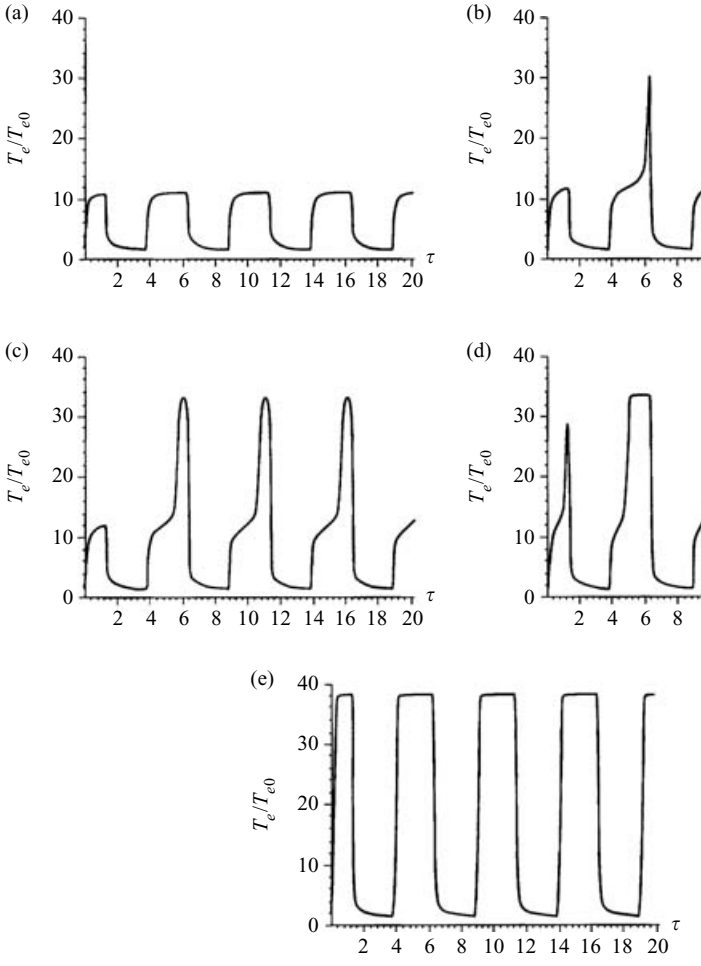


**Figure 5.** Electron temperature $T_e(\tau)$ enhanced and modulated by using five different normalized heating powers: (a) $p = 5.8$, (b) $p = 5.87$, (c) $p = 5.89$, (d) $p = 6$ and (e) $p = 8$.

at a constant level after the initial increase in the interval from 10 to 100 Hz. While that produced by the half-wave rectified wave scheme has a peak at 1000 Hz in its distribution. These results demonstrate that the half-wave rectified wave scheme is the most efficient one and the sine wave scheme produces the best quality ELF/VLF signals for communications.

*5.2. Dependence of the radiation intensity on the heating power* (*thermal instability*)

We now study the dependence of the radiation intensity on the X-mode heating power. Power modulation by rectangular wave at modulation frequency $f_1 = 100$ Hz is first considered. Thus, $M(\tau) = 1 + 4\sum_{n=0}(-1)^n \cos[(2n+1)\omega_{10}\tau]/(2n+1)\pi$ and $q = 0.03pM(\tau)$, where $\omega_{10} = 0.4\pi$ and $p$ is the only variable parameter left in (21). It is noted that the considered power modulation function $M(\tau)$ contains no even harmonic components. Presented in Fig. 5 are the electron temperature $T_e(\tau)$ for the five cases where $p = 5.8$, 5.87, 5.89, 6 and 8. As shown in Fig. 5(a) for $p = 5.8$, the electron temperature quickly reaches the steady

https://doi.org/10.1017/S0022377802001964 Published online by Cambridge University Press

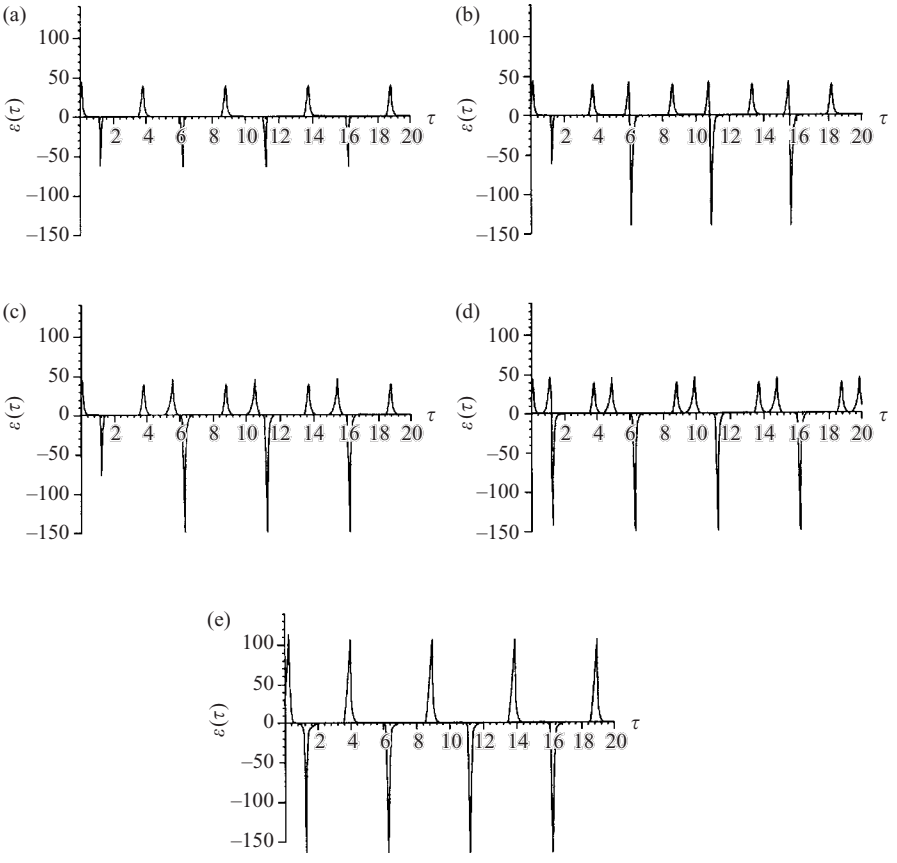


**Figure 6.** Radiation fields $\varepsilon(\tau)$ in (a)–(e) corresponding to the five cases presented in Fig. 5.

state in a rectangular waveform with considerable DC enhancement as well as AC modulation. As $p$ increases slightly to $p = 5.87$, as shown in Fig. 5(b) a sudden change in functional features is observed. The electron temperature modulation function evolves quickly from a rectangular waveform (similar to that in Fig. 5a) to one having an additional spike enhanced by about 4.8 dB. As $p$ increases to 5.89, the spike in (b) is widened, manifesting a transition of the electron temperature in each modulation pulse from one steady-state level to a much higher steady-state level (about 5 dB enhancement) as shown in Fig. 5(c). At this heating power level the passive Ohmic heating process for the electrojet modulation is no longer a dominant process. The plasma nonlinearity and thermal instability become major processes in the electrojet modulation. With a further increase of the heating power level to a critical value $p = 6$, the electron temperature modulation evolves directly, as shown in Fig. 5(d), to the higher steady-state level, which again depends weakly on the heating power, as demonstrated by the temperature function shown in Fig. 5(e) for a considerable increase of the heating power level to $p = 8$. In this case, the stimulated thermal instability becomes the dominant electrojet modulation process. The time functions of the radiation fields $\varepsilon(\tau)$ for the same five cases are presented in Figs 6(a)–(e). As shown, consistently, a sudden change in the function form also occurs in the same heating power regime.

https://doi.org/10.1017/S0022377802001964 Published online by Cambridge University Press

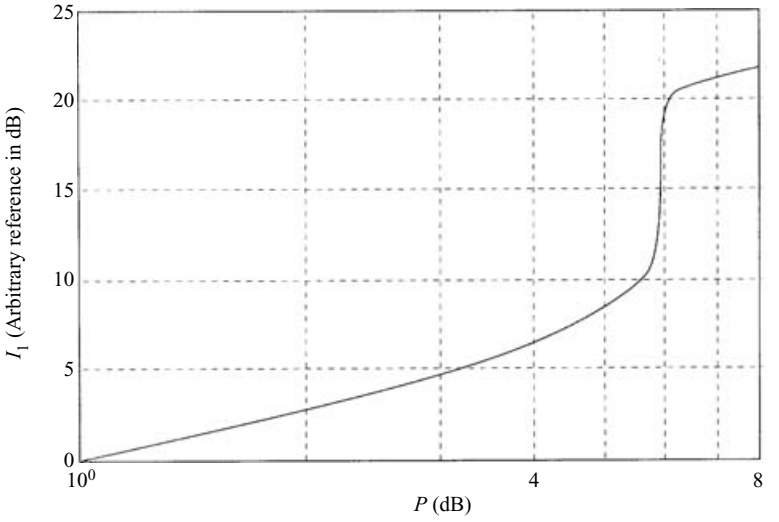


**Figure 7.** The dependence of the spectral intensity $I_1$ of the fundamental line of the radiation on the normalized heating power $p$, which shows a (near) step increase in the spectral intensity as the heating power exceeds a threshold $p_c = 6$ with a modulation frequency $f_1 = 100$ Hz.

We have found, as demonstrated in Figs 5 and 6, that when the heating power passes a narrow transition region to exceed a threshold level, there is a sudden increase in the electron temperature and the radiation intensity. Stimulated thermal instability becomes the dominant electrojet heating and modulation process. It has a much higher saturation level. The dependence of the spectral intensity $I_1$ of the fundamental radiation line, for the $f_1 = 100$ Hz case, on the normalized heating power $p$ is presented in Fig. 7. It is shown that this function has a narrow transition region of width $\Delta p$. As $p$ passes this transition region to exceed a threshold value $p_c$, the spectral intensity of the signal is suddenly increased by more than 10 dB from that with a $p$ slightly less than $p_c$. The threshold value $p_c$ varies with the modulation frequency $f_1$. Similar calculations have been carried out for different modulation frequencies in the range from 10 to 500 Hz. This dependence, showing a monotonic increase of the threshold value $p_c$ with the modulation frequency $f_1$, is presented in Fig. 8. The numerical results also show that the width $\Delta p$ of the transition region increases and $I_1$ increases across the transition region, $\Delta I_1$, and decreases as the modulation frequency $f_1$ increases. The dependence of the ratio $\Delta I_1/\Delta p$ on $f_1$ is presented in Fig. 9, in which $\partial I_1(p, f_1)/\partial p|_p = 1$ is also presented for comparison. The slope in the transition region is much larger than that at $p = 1$ (as well as that for $p < p_c$), representing a considerable increase in the generation efficiency. The improvement in the generation efficiency, however, goes down as the modulation frequency increases.

It is noted that the dependence of the signal intensity on the heating power has been investigated previously (Papadopoulos et al. 1990). But the phenomenon of a (near) step increase of the radiation intensity was not found in simulation results. This was because the heating power used in the simulation study was below the threshold level.

https://doi.org/10.1017/S0022377802001964 Published online by Cambridge University Press

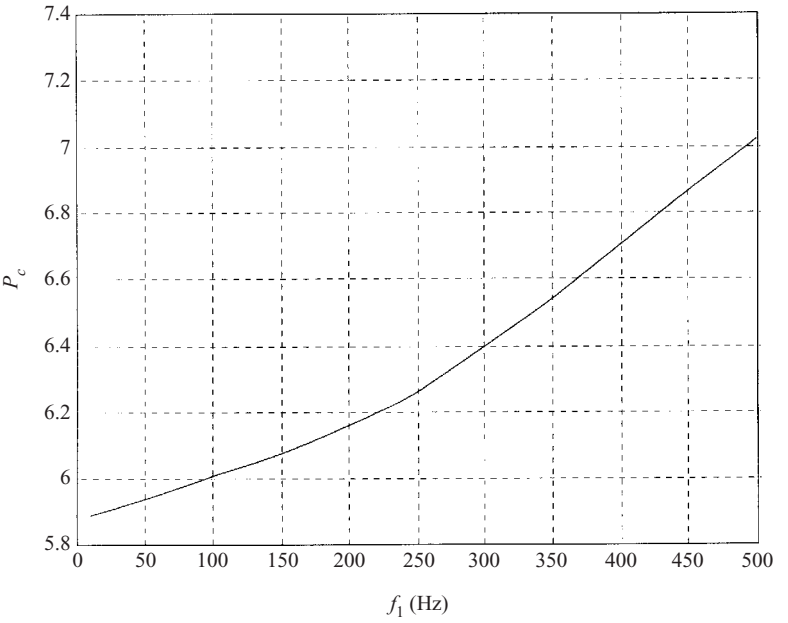


**Figure 8.** The dependence of the threshold power $p_c$ on the modulation frequency $f_1$.

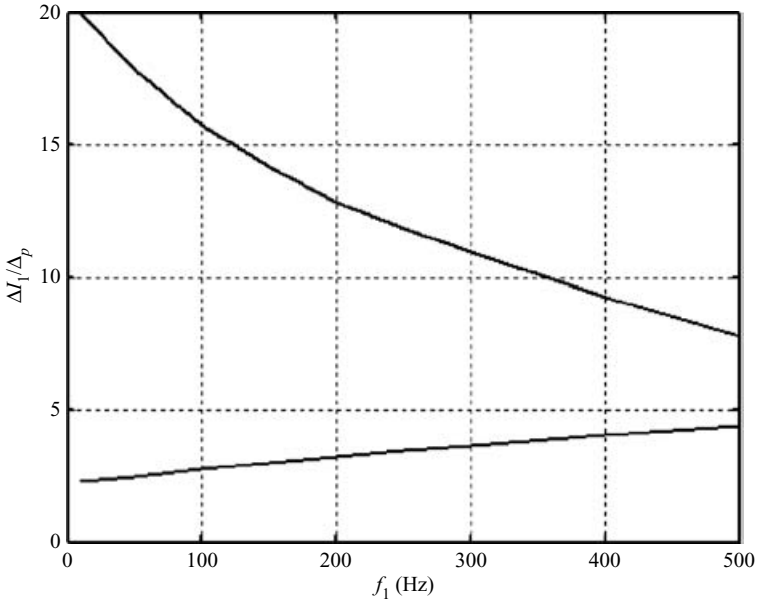


**Figure 9.** The dependence of the ratio $\Delta I_1/\Delta p$, the increase rate of the spectral intensity $I_1$ in the major enhancement region, on the modulation frequency $f_1$. The slope of $I_1(p, f_1)$ at $p = 1$, which is the one close to the horizontal axis, is also presented for comparison.

https://doi.org/10.1017/S0022377802001964 Published online by Cambridge University Press

## 6. Discussion and conclusion

Using an amplitude-modulated HF heating wave, the polar electrojet current is modulated to act as a virtual ionospheric antenna for ELF wave generation. The current modulation is the result of time-dependent heating of background electrons, which modulates the electrojet conductivity accordingly.

One approach to improving the modulation efficiency is to employ a proper amplitude-modulation method on HF heating waves. The numerical results presented in Figs 3 and 4 show that the sine wave scheme generates the best quality signal, which has the lowest second harmonic content, and the half-wave rectified wave modulation scheme is the most efficient one for generating a signal at the modulation frequency.

Since the electron-heating rate increases with electron temperature (as shown by the first term on the RHS of (6) and (21)), a stimulated thermal instability is also excited by the amplitude-modulated HF heating wave in the electrojet. This instability leads the transient temperature response of electrojet plasma to grow exponentially at the expense of the free energy of the heating wave (the second term in the brackets of the first term on the RHS of (6)) as well as the background electrojet current (the first term in the brackets of the first term on the RHS of (6)). The result shows that this instability can, in fact, be a dominant process of electron temperature modulation before the nonlinear damping of inelastic collisions stabilizes it. Inelastic collisions of electrons with neutral particles (mainly due to vibration excitation of $N_2$) introduce nonlinear damping which stabilizes the instability. The nonlinear damping rate $\mu_I$ on the LHS of (21) turns out to become a rapidly decreasing function of $\chi$ after reaching a peak at $\chi \cong 10$. Numerical analysis then confirms that as the power of the HF heating wave exceeds a threshold level, a significant electron heating can occur, which causes a steep drop in the electron inelastic collision rate. This stimulated instability is thus saturated at a much higher level, resulting in a (near) step enhancement (of about 10 dB) in the generation efficiency of ELF radiation. However, the threshold power is rather high. For example, the threshold field, for using a 4 MHz X-mode heating wave modulating at 100 Hz, is about 6.1 V m$^{-1}$, determined from the plot in Fig. 8. This threshold field is also modulation-scheme-dependent. It reduces to 4.4 V m$^{-1}$ as a half-wave rectified-wave modulation scheme, with $M(\tau) = 1 - (16/\pi) \sum_{k=1} [(\sin k\pi/2)/k(k^2-4)] \cos k(\omega_{10}\tau - \pi/2)$, is applied. This modulation scheme also advantageously increases the (near) step jump in the radiation intensity to 13 dB. Without considering the absorption of the HF power by the D region ionosphere, this threshold power (having an effective radiated power ERP slightly greater than 90 dBW) evaluated for the E region parameters ($\sim$ 100 km altitude) already exceeds the maximum available power of the European Incoherent Scatter facility's superheater (Stubbe 1996) in Tromso, Norway. Such absorption of the HF power by the D region ionosphere during daytime or under disturbed conditions could severely reduce the HF power transmitted to altitudes near 100 km. This further increases the required power of HF heaters to take advantage of the thermal instability for effective E region electrojet modulation. Nevertheless, this extraordinary physical phenomenon could well be explored in future heating experiments by a further upgraded EISCAT superheater under favourable ionospheric conditions, or by the High Frequency Active Auroral Research Program (HAARP) heating facility (Kossey et al. 1999) in Gakona, Alaska when its effective radiated power reaches its planned level.

*Acknowledgements*

I am grateful to M. C. Lee, Paul Kossey, Lee Snyder, John Heckscher and Edward Kennedy for helpful discussions, and to S. H. Lee for the numerical work. This work was supported by the High Frequency Active Auroral Research Program (HAARP), Air Force Research Laboratory at Hanscom Air Force Base, Massachusetts and by the Office of Naval Research Grant ONR-N00014-00-1-0938. Part of the financial support of this work was from NorthWest Research Associates, Inc.

## References

Barr, R. and Stubbe, P. 1984a *J. Atmos. Terr. Phys.* **46**, 315.

Barr, R. and Stubbe, P. 1984b *Radio Sci.* **19**, 1111.

Barr, R. and Stubbe, P. 1991a *Geophys. Res. Lett.* **18**, 1971.

Barr, R. and Stubbe, P. 1991b *Geophys. Res. Lett.* **18**, 1035.

Barr, R., Stubbe, P. and Kopka, H. 1991 *Radio Sci.* **26**, 871.

Braginskii, S. I. 1965 Transport processes in a plasma. In: *Reviews of Plasma Physics* Vol. 1 (ed. M. A. Loentovid). New York: Consultant's Bureau.

Ferraro, A. J., Lee, H. S., Allshouse, R., Carroll, K., Tomko, A. A., Kelly, F. J. and Joiner, R. G. 1982 *J. Atmos. Terr. Phys.* **44**, 1113.

Ferraro, A. J., Lee, H. S., Allshouse, R., Carroll, K., Lunnen, R. and Collins, T. 1984 *J. Atmos. Terr. Phys.* **46**, 855.

Gurevich, V. A. 1978 *Nonlinear Phenomena in the Ionosphere*. New York: Springer-Verlag, Chap. 2.

James, H. G., Dowden, R. L., Rietveld, M. T., Stubbe, P. and Kopka, H. 1984 *J. Geophys. Res.* **89**, 1655.

Kossey, P., Heckscher, J., Carlson, H. and Kennedy, E. 1999 HAARR – High Frequency Active Auroral Research program. *J. Arctic Res. US*. Washington, DC: National Science Foundation.

Kuo, S. P. 1993 *Radio Sci.* **28**, 1019.

Kuo, S. P. and Lee, M. C. 1983 *Geophys. Res. Lett.* **10**, 979.

Kuo, S. P. and Lee, M. C. 1993 *Geophys. Res. Lett.* **20**, 189.

Kuo, S. P., Faith, J., Lee, M. C. and Kossey, P. 1998 *J. Geophys. Res.* **103**, 4063.

Kuo, S. P., Lee, M. C., Kossey, P., Groves, K. and Heckscher, J. 2000 *Geophys. Res. Lett.* **27**, 85.

Kuo, S. P., Lee, S. H. and Kossey, P. 2002 *Phys. Plasmas* **9**.

Lee, H. S., Ferraro, A. J. and Olson, J. V. 1990 *Radio Sci.* **25**, 1429.

McCarrick, M. J., Sentman, D. D., Wong, A. Y., Wuerker, R. F. and Chouinard, B. 1990 *Radio Sci.* **25**, 1291.

Papadopoulos, K. and Chang, C. L. 1985 *Geophys. Res. Lett.* **12**, 279.

Papadopoulos, K., Chang, C. L., Vitello, P. and Drobot, A. 1990 *Radio Sci.* **25**, 1311.

Rietveld, M. T., Kopka, H. and Stubbe, P. 1986 *J. Atmos. Terr. Phys.* **48**, 311.

Rietveld, M. T., Stubbe, P. and Kopak, H. 1989 *Radio Sci.* **24**, 270.

Stubbe, P. 1996 *J. Atmos. Terr. Phys.* **58**, 349.

Stubbe, P. and Kopka, H. 1977 *J. Geophys. Res.* **82**, 2319.

Stubbe, P., Kopka, H. and Dowen, R. L. 1981 *J. Geophys. Res.* **86**, 9073.

Stubbe, P., Kopka, H., Rietveld, M. T. and Dowen, R. L. 1982 *J. Atmos. Terr. Phys.* **44**, 1173.

Stubbe, P., Kopka, H., Rietveld, M. T., Frey, A., Hoeg, P., Kohl, H., Nielsen, E. and Rose, G. 1985 *J. Atmos. Terr. Phys.* **47**, 1151.

Villasenor, J., Wong, A. Y., Song, B., Pau, J., M. J. McCarrick and Sentman, D. D. 1996 *Radio Sci.* **31**, 1.